Three-dimensional numerical simulation of an equilateral triangular turbulent free jet

Keivan Khademi Shamami and Madjid Birouk
Department of Mechanical and Manufacturing Engineering, The University of Manitoba, Winnipeg, Manitoba, Canada

Received 30 January 2008
Revised 28 July 2008
Accepted 12 August 2008

Abstract

Purpose – This paper aims to describe the numerical simulation of a three-dimensional turbulent free jet issuing from a sharp-edged equilateral triangular orifice into still air.

Design/Methodology/approach – The numerical simulation was carried out by solving the governing three-dimensional Reynolds-averaged Navier-Stokes equations. Several two-equation eddy-viscosity models (i.e. the standard k-ε, renormalization group (RNG) k-ε, realizable k-ε, shear-stress transport (SST) k-ω), as well as the Reynolds stress models (i.e. the standard RSM and the SSG) were tested to simulate the flowfield. The numerical predictions were compared with experimental data in order to assess the capability and limitations of the various turbulent models examined in this work.

Findings –The vena contracta effect was predicted by all the tested models. Among the eddy-viscosity models only the realizable k-ε model showed good agreement of the near-field jet decay. None of the eddy-viscosity models was capable of predicting the profiles of the jet turbulence intensities. The RSMs, especially the standard RSM, were able to produce much better predictions of the features of the jet in comparison with the eddy-viscosity models. The standard RSM predictions were found to agree reasonably well with the experimental data.

Research limitations/implications – The conclusion, that among the tested RANS turbulence closure models, the RSM appeared the only one capable of reproducing reasonably well the experimental data concerns only the jet flow case examined here. Also, the average computational time for a single run was quite long, i.e. 340 h, but it is believed that parallel computing will reduce it considerably.

Originality/value – The numerical results reported in this paper provide a comparison between several RANS turbulence closure models for simulating a turbulent free jet issuing from an equilateral triangular nozzle.

Keywords Free jet, Jets, Simulation, Structural analysis, Turbulence
Paper type Research paper

Nomenclature

b_{ij}	Reynolds stress anisotropic tensor
B_e	geometric mean of the jet half-velocity widths
C_1, C_2	RSMs constants
C_3, C_4, C_5	SSG model constants
C_1^*, C_3^*	SSG model constants
C_1', C_2'	standard RSM constants
$C_{1\varepsilon}, C_{2\varepsilon}, C_\mu$	k-ε based models constants and RSMs constants
D_e	equivalent diameter of the triangular orifice
D_{ij}	diffusion term of Reynolds stress transport equation

The authors would like to greatly acknowledge the financial support for this research by Manitoba Hydro Research and Development Department, Project Monitor Mr Nick Read. The authors would like to thank also Dr W. Quinn, Professor of Engineering at St. Francis Xavier University, for providing the experimental data which were used for comparison in the present paper.

International Journal of Numerical Methods for Heat & Fluid Flow
Vol. 19 No. 7, 2009
pp. 894-912

0961-5539
DOI 10.1108/09615530910984136

k	turbulence kinetic energy
l	turbulence length scale
P	pressure
P_{ij}	production term of Reynolds stress transport equation
S_{ij}	mean rate of strain tensor
u_i, u_j, u_k	velocity fluctuation components
$\overline{u_i u_j}$	Reynolds stresses
U_i, U_j, U_k	mean-velocity components
U_{cl}	local streamwise mean velocity on the jet centerline
U_{max}	maximum value of the streamwise mean velocity on the jet centerline
x	axial distance to the orifice exit plane
y,z	lateral distances from jet centerline
$Y_{1/2}$	jet half-velocity width in the central x-y plane
$Z_{1/2}$	jet half-velocity width in the central x-z plane

Greek letters

Ω_{ij}	mean vorticity tensor
δ_{ij}	Kronecker operator
ε	rate of dissipation of k
ε_{ij}	dissipation term of Reynolds stress transport equation
Φ_{ij}	pressure-strain term of Reynolds stress transport equation
$\phi_{ij,1}$	return-to-isotropy term in the pressure-strain term (Φ_{ij})
$\phi_{ij,2}$	rapid pressure-strain term in the pressure-strain term (Φ_{ij})
$\phi_{ij,w}$	wall-reflection term in the pressure-strain term (Φ_{ij})
μ	dynamic viscosity
μ_t	eddy viscosity
ρ	density
$\sigma_k, \sigma_\varepsilon$	k-ε based models constants and RSMs constants
ν	kinematic viscosity
ω	specific dissipation Rate

1. Introduction

Free jets issuing from non-circular nozzles have advantages over their conventional axisymmetric counterparts. The use of nozzles with, for example, triangular-, rectangular-, and square-shaped exit orifice were found to promote large-scale mixing which enhances bulk reactants mixing, and small-scale mixing at molecular level to initiate chemical reactions. It was shown that these types of nozzles generate large-scale mixing at the flat sides of the nozzle and small-scale mixing at the corners (e.g. Quinn, 2005a, b; Schadow *et al.*, 1988).

A review of current literature revealed that numerous experimental studies were performed on free jets issuing from non-circular nozzles and orifices with sharp edges (e.g. Iyogun and Birouk, 2008, 2009; Quinn, 1990, 1992, 1994, 2005a, b, c; Mi *et al.*, 2000, 2005; Zaman, 1995, 1996, 1999; Vandsburger and Ding, 1995; Liu and Wu, 1995; Rice and Raman, 1993; Gutmark *et al.*, 1989a, b, 1991; Grandmaison *et al.*, 1991; Tsuchiya *et al.*, 1989; Schadow *et al.*, 1988; Krothapalli *et al.*, 1981; Marsters, 1981; Sfeir, 1979; Sforza *et al.*, 1966). These types of jets were also the subject of several numerical studies. Rectangular and square free jets received most of the attention (e.g. Berg *et al.*, 2006; de With and Holdo, 2005; Imine *et al.*, 2004; Wilson and Imber, 2003; Rembold *et al.*, 2002; Abdel-Hameed and Bellan, 2002; Jiang and Luo, 2001; Reddy *et al.*, 1998, 1999; Wilson and Demuren, 1998; Grinstein, 1998; Zaman *et al.*, 1997; Grinstein and DeVore,

1996; Miller *et al.*, 1995; Grinstein and Kailasanath, 1995; Teshima, 1989; Quinn and Militzer, 1988). However, only a few numerical studies were devoted to triangular jets (Imine *et al.*, 2004; Abdel-Hameed and Bellan, 2002; Miller *et al.*, 1995). Literature up to 1997 concerning non-circular jets was reviewed by Gutmark and Grinstein (1999). Also, a short review of experimental and numerical studies on triangular jets up to 2005 was reported by Quinn (2005a, b). A brief review of numerical studies which dealt with free jets issuing from triangular nozzles (or orifices) is reported below.

Miller *et al.* (1995) performed direct numerical simulation to study three-dimensional jets issuing from circular and non-circular nozzles of identical equivalent diameters at a Reynolds number of 800, which is based on the nozzle equivalent diameter and the relative exit velocity between the co-flowing stream and the jet. They tested elliptic, square, rectangular, equilateral triangular, and isosceles triangular nozzles. They reported that the triangular jets showed markedly different characteristics than the other tested jets. They reported that coherent large-scale structures were quickly masked by the small-scale structures formed at the corners, and more importantly a non-circular jet (especially the triangular jet) was found to promote better mixing than does a circular jet. Abdel-Hameed *et al.* (2002) also performed direct numerical simulations to study the characteristics of three-dimensional, laminar free jets issuing from different inlet geometric configurations (i.e. circular, elliptic, rectangular, square, and triangular). For both single-phase and two-phase flows, it was shown that the square geometry appeared to enhance only marginally the entrainment rate compared with the circular jet. On the other hand, the rectangular, elliptic, and triangular jets exhibited substantial enhancement in entrainment. It is also reported that the triangular jet displayed the largest fine-scale production at the vertices. Imine *et al.* (2004) investigated numerically the effects of the nozzle orifice geometry on the process of jet mixing, in which rectangular, elliptic, and triangular pipes with an aspect ratio of 1.33 were considered. A second-order Reynolds stress model (RSM) was then used to investigate the flowfield of asymmetric turbulent free jets. It was reported that the asymmetric geometries enhanced the mixing in comparison with their axisymmetric counterparts. The rectangular jet showed the fastest centerline streamwise mean-velocity decay rate, followed by the elliptic and the triangular jets.

These numerical studies are consistent with previous findings in concluding that jet flows issuing from nozzles with asymmetric nozzles tend to promote better mixing than their axisymmetric counterpart. In addition, there are very few comparisons of numerical results with experimental data to validate the accuracy of the numerical simulations, particularly for jets issuing from a triangular-shaped nozzle. Therefore, the aim of the present study is to provide an analysis of the performance of several RANS turbulence closure models, and thus verify their ability in predicting the main characteristics of a turbulent free jet issuing from a sharp-edged equilateral triangular orifice. The predictions are compared with their experimental counterparts.

2. Computational details

2.1 Physical problem

The physical problem consists of a free jet of air injected into still atmosphere of air from an equilateral triangular orifice. The jet, which is assumed steady, incompressible and isothermal, and its surrounding air are considered having the same (room) temperature.

2.2 Governing equations

The governing mass and momentum Reynolds-averaged equations for a turbulent steady-state flow can be written in tensor notation as follows:

$$\frac{\partial(\rho U_i)}{\partial x_i} = 0 \tag{1}$$

$$\frac{\partial(\rho U_i U_j)}{\partial x_j} = -\frac{\partial P}{\partial x_i} + \frac{\partial}{\partial x_i}\left(\mu\frac{\partial U_i}{\partial x_j} - \rho\overline{u_i u_j}\right) \tag{2}$$

The time-averaged velocity fluctuating tensors, $\overline{u_i u_j}$, also called the Reynolds stresses, are unknown. The numerical solution of Equations (1) and (2) for a turbulent flow can be obtained only by introducing additional equations for the Reynolds stresses. These equations contain other correlations of higher order which have to be modeled in order to close the system of Reynolds-averaged equations.

2.3 Turbulence closure models

The turbulence models tested here are grouped into two families: (i) the two-equation eddy-viscosity models, which are the k-ε, renormalization group (RNG) k-ε, realizable k-ε, and the shear-stress transport (SST) k-ω, and (ii) the RSMs, which are the standard RSM and the SSG. These models are summarized briefly below.

2.3.1 k-ε model. For k-ε model, the Reynolds stresses are linearly related to the mean rate of strain by a scalar eddy viscosity as follows (Launder and Spalding, 1974):

$$-\rho\overline{u_i u_j} = 2\mu_t S_{ij} - \frac{2}{3}\rho k\delta_{ij} \tag{3}$$

where S_{ij} and μ_t are the mean rate of strain tensor and the eddy viscosity which are given, respectively, as

$$S_{ij} = \frac{1}{2}\left(\frac{\partial U_i}{\partial x_j} + \frac{\partial U_j}{\partial x_i}\right) \tag{4}$$

$$\mu_t = C_\mu\rho\frac{k^2}{\varepsilon} \tag{5}$$

where k and ε are the turbulence kinetic energy and dissipation rate, respectively, which are expressed as

$$k = \frac{1}{2}\overline{u_i u_i} \tag{6}$$

$$\varepsilon = \nu\overline{\frac{\partial u_i}{\partial x_j}\frac{\partial u_i}{\partial x_j}} \tag{7}$$

The k-ε model (called KEM in the present study), consists of the following transport equations for k and ε, respectively

$$\frac{\partial(\rho U_j k)}{\partial x_j} = \frac{\partial}{\partial x_j}\left((\mu + \frac{\mu_t}{\sigma_k})\frac{\partial k}{\partial x_j}\right) + 2\mu_t S_{ij}S_{ij} - \rho\varepsilon \tag{8}$$

$$\frac{\partial(\rho U_j \varepsilon)}{\partial x_j} = \frac{\partial}{\partial x_j}\left((\mu + \frac{\mu_t}{\sigma_\varepsilon})\frac{\partial \varepsilon}{\partial x_j}\right) + 2C_{1\varepsilon}\frac{\varepsilon}{k}\mu_t S_{ij} S_{ij} - C_{2\varepsilon}\rho\frac{\varepsilon^2}{k} \tag{9}$$

The model constants, which are determined from experiments for homogeneous shear flows and isotropic grid turbulence (Launder and Spalding, 1972), are summarized in Table I.

2.3.2 RNG k-ε model. The RNG-based k-ε model (called RNG in the present study), is derived by using a mathematical technique called the "RNG" method (Yakhot and Orszag, 1986). It has a similar form to the KEM. The main difference between the RNG and standard k-ε models is the additional term in the ε-equation of the RNG model.

The additional term which is subtracted from the right hand side of Equation (9) to derive the ε transport equation in the RNG model is defined as

$$R_\varepsilon = \frac{C_\mu \rho \eta^3 (1 - \eta/\eta_0)}{1 + \beta\eta^3}\frac{\varepsilon^2}{k} \tag{10}$$

where $\eta = \sqrt{2S_{ij}S_{ij}}k/\varepsilon$, $\eta_o = 4.38$, and $\beta = 0.012$. The model constants, which are summarized in Table I, are obtained analytically (Yakhot *et al.*, 1992). A more comprehensive description of the RNG can be found in Choudhury (1993).

2.3.3. Realizable k-ε model. The realizable k-ε model (called RKEM in the present study), proposed by Shih *et al.* (1995), has a new eddy-viscosity equation, as well as a new dissipation equation. The k-equation in the RKEM model has the same form used in the KEM and RNG models; however, a different ε-equation is employed

$$\frac{\partial(\rho\varepsilon)}{\partial t} + \frac{\partial(\rho U_j \varepsilon)}{\partial x_j} = \frac{\partial}{\partial x_j}\left((\mu + \frac{\mu_t}{\sigma_\varepsilon})\frac{\partial \varepsilon}{\partial x_j}\right) + \rho C_1\sqrt{2S_{ij}S_{ij}}\varepsilon - \rho C_2\frac{\varepsilon^2}{k + \sqrt{\varepsilon\upsilon}} \tag{11}$$

where

$$\mathrm{C}_1 = \max\left[0.43, \frac{\eta}{\eta + 5}\right] \tag{12}$$

The turbulent viscosity is computed using Equation (5), however, C_μ is not a constant and is calculated using the following equation:

$$C_\mu = \frac{1}{A_0 + A_s(kU^*/\varepsilon)} \tag{13}$$

	C_μ	$\mathrm{C}_{1\varepsilon}$	$\mathrm{C}_{2\varepsilon}$	σ_k	σ_ε
KEM	0.09	1.44	1.92	1	1.3
RNG	0.0845	1.42	1.68	0.7179	0.7179
RKEM	–	1.44	1.9	1	1.2

Table I.
k-ε based models coefficients

where

$$U^* = \sqrt{S_{ij}S_{ij} + \vec{\Omega}_{ij}\vec{\Omega}_{ij}} \tag{14}$$

$$\vec{\Omega}_{ij} = \Omega_{ij} - 2\varepsilon_{ijk}\omega_k\,, \quad \Omega_{ij} = \frac{1}{2}\left(\frac{\partial \overline{u}_i}{\partial x_j} - \frac{\partial \overline{u}_j}{\partial x_i}\right) \tag{15}$$

$$\mathrm{A}_0 = \text{Constant}\,, \quad \mathrm{A}_\mathrm{s} = \sqrt{6}\cos\phi \tag{16}$$

$$\phi = \frac{1}{3}\cos^{-1}(\sqrt{6}W)\,, \quad W = \frac{S_{ij}S_{jk}S_{ki}}{\vec{S}^3}\,, \quad \vec{S} = \sqrt{S_{ij}S_{ij}} \tag{17}$$

The model constants are given in Table I.

2.3.4 SST k-ω model. The shear-stress transport k-ω model (called SST in the present study), developed by Menter (1994), is a modification of the standard k-ω model where the equation for the turbulent viscosity is modified to account for the transport of the principal turbulent shear stress (Menter, 1994). The detailed model description and model constants can be found in Menter (1994) and Menter *et al.* (2003).

2.3.5 Reynolds stress model (RSM). In the RSM, the Reynolds stresses are calculated from their transport equations (Launder *et al.*, 1975). Closure for Reynolds stresses require six equations for the six independent Reynolds stresses, $\overline{u_i u_j}$, and another equation for the isotropic turbulence energy dissipation rate, ε. The Reynolds stress transport equations are expressed as

$$\frac{\partial}{\partial t}(\rho\overline{u_i u_j}) + \frac{\partial}{\partial x_k}(\rho U_k \overline{u_i u_j}) = D_{ij} + P_{ij} + \phi_{ij} - \varepsilon_{ij} \tag{18}$$

where $D_{ij}, P_{ij}, \phi_{ij}$, and ε_{ij} represent, respectively, the diffusion, production, pressure-strain, and viscous dissipation.

It should be noted that in the present study, instead of using the generalized gradient-diffusion model of Daly and Harlow (1970) for the D_{ij} term, the simplified model equation reported by Lien and Leschziner (1994) is used, which is expressed as

$$D_{ij} = \frac{\partial}{\partial x_k}\left(\frac{\mu_t}{\sigma_k}\frac{\partial \overline{u_i u_j}}{\partial x_k}\right) \tag{19}$$

The pressure-strain term has been modeled using the three-term relationship (Gibson and Launder, 1978; Fu *et al.*, 1987; Launder, 1989a, b)

$$\phi_{ij} = \phi_{ij,1} + \phi_{ij,2} + \phi_{ij,w} \tag{20}$$

where $\phi_{ij,1}$ is the return-to-isotropy term, $\phi_{ij,2}$ is the rapid pressure-strain term, and $\phi_{ij,w}$ is the wall-reflection term. The three components of the pressure-strain term are modeled as

$$\phi_{ij,1} = -C_1\rho\frac{\varepsilon}{k}\left[\overline{u_i u_j} - \frac{2}{3}\delta_{ij}k\right] \tag{21}$$

$$\phi_{ij,2} = -C_2\left[(P_{ij} - C_{ij}) - \frac{1}{3}\delta_{ij}(P_{kk} - C_{kk})\right] \tag{22}$$

$$\phi_{ij,w} = C_1' \frac{\varepsilon}{k}\left[\overline{u_k u_m} n_k n_m \delta_{ij} - \frac{3}{2}\overline{u_i u_k} n_j n_k - \frac{3}{2}\overline{u_j u_k} n_i n_k\right]\frac{k^{3/2}}{C_l \varepsilon d} + C_2'\left[\phi_{km,2} n_k n_m \delta_{ij} - \frac{3}{2}\phi_{ik,2} n_j n_k - \frac{3}{2}\phi_{jk,2} n_i n_k\right]\frac{k^{3/2}}{C_l \varepsilon d} \quad (23)$$

where

$$P_{ij} = -\rho\overline{u_i u_k}\frac{\partial U_j}{\partial x_k} - \rho\overline{u_j u_k}\frac{\partial U_i}{\partial x_k}, \quad C_{ij} = \frac{\partial \rho U_k \overline{u_i u_j}}{\partial x_k} \quad (24)$$

and n_k is the x_k component of the unit normal to the wall, d is the normal distance to the wall, $C_l = C_\mu^{3/4}/\kappa$, and κ is the von Karman constant (=0.4187). The turbulence energy dissipation rate, ε, is obtained by solving the following transport equation:

$$\frac{\partial(\rho\varepsilon)}{\partial t} + \frac{\partial(\rho\varepsilon U_i)}{\partial x_i} = \frac{\partial}{\partial x_j}\left[(\mu + \frac{\mu_t}{\sigma_\varepsilon})\frac{\partial \varepsilon}{\partial x_j}\right] + \frac{1}{2}C_{\varepsilon 1}\frac{\varepsilon}{k}P_{ii} - C_{\varepsilon 2}\rho\frac{\varepsilon^2}{k} \quad (25)$$

The model constants are reported in Table II.

2.3.6 Quadratic pressure-strain (SSG) model. The SSG uses a quadratic pressure-strain model instead of a linear pressure-strain model (Speziale *et al.*, 1991). It is expressed as

$$\phi_{ij} = -(C_1\varepsilon + C_1^* P)b_{ij} + C_2\varepsilon(b_{ik}b_{kj} - \frac{1}{3}b_{mn}b_{mn}\delta_{ij}) + (C_3 - C_3^*\sqrt{b_{ij}b_{ij}})kS_{ij} + C_4\,k(b_{ik}S_{jk} + b_{jk}S_{ik} - \frac{2}{3}b_{mn}S_{mn}\delta_{ij}) + C_5\,k(b_{ik}\Omega_{jk} + b_{jk}\Omega_{ik}) \quad (26)$$

where b_{ij} is the Reynolds stress anisotropy tensor given as

$$b_{ij} = \frac{\overline{u_i u_j}}{2k} - \frac{1}{3}\delta_{ij} \quad (27)$$

where S_{ij} and Ω_{ij} are the mean rate of the strain tensor and the mean vorticity tensor, respectively, which are defined as

$$S_{ij} = \frac{1}{2}\left(\frac{\partial U_j}{\partial x_i} + \frac{\partial U_i}{\partial x_j}\right), \quad \Omega_{ij} = \frac{1}{2}\left(\frac{\partial U_i}{\partial x_j} - \frac{\partial U_j}{\partial x_i}\right) \quad (28)$$

The model constants are tabulated in Table II.

Table II. Reynolds stress models coefficients

	C_μ	C_1	C_1*	C_2	C_3	C_3*	C_4	C_5	$C_{1\varepsilon}$	$C_{2\varepsilon}$	C'_1	C'_2	σ_k	σ_ε
RSM	0.09	1.8	–	0.6	–	–	–	–	1.44	1.92	0.5	0.3	1	1.3
SSG	0.09	3.4	1.8	4.2	0.8	1.3	1.25	0.4	1.44	1.83	–	–	1	1.3

2.4 Numerical solution

The set of equations, which result from Equation (2), are solved by the aid of the turbulence closure models described in the previous section. The triangular orifice and the computational domain are schematically shown in Figure 1.

The test conditions are set as follows. The streamwise mean velocity at the center of the orifice exit plane is 61 m/s, which corresponds to a Reynolds number of 1.84×10^5 based on the orifice equivalent diameter ($D_e = 45.3$ mm). This choice is based on the experimental data provided by Quinn (2005a). Note that experimental data are available starting from $x/D_e = 0.5$ downstream of the orifice exit plane. Therefore, the experimental data at this nearest location to the nozzle exit are used as the inlet boundary conditions. The experimental data for the turbulence kinetic energy (k) at $x/D_e = 0.5$ are used as the inlet boundary condition for k. The dissipation rate of the turbulence kinetic energy (ε) at the inlet is calculated by $\varepsilon = C_\mu^{3/4} k^{3/2}/l$, where C_μ is a constant (=0.09), k is the turbulence kinetic energy, and l is the turbulence length scale which can be approximated as $0.33D_e$ (Mahmud *et al.*, 2007). The computational domain is chosen to be long enough to ensure complete development of the flow; that is, up to $x/D_e = 120$. In the lateral sides, i.e. y and z directions, the computational domain is 80*De* wide. At the outlet and at the four lateral planes, a zero gradient along the normal vector of the planes is assumed for all the variables (i.e. *U, V, W, P*, etc.). A two-layer-based, non-equilibrium wall function (Kim and Choudhury, 1995) is used near the wall. In this model, the log-law of Launder and Spalding (Launder and Spalding, 1974) for the mean velocity is sensitized to the effects of pressure gradient, and it is also assumed that the wall-neighboring cells consist of a viscous sublayer and a fully turbulent layer (FLUENT, 2005). In the present work, the centroid for the cell adjacent to the wall is located at $y^+ (= U_\tau y/\nu) \approx 45$.

Grid independency was verified by using several different mesh sizes. The coarsest grid, which consisted of $96 \times 78 \times 78$ (in the axial, x, and lateral, y and z, directions, respectively) was chosen to be the mesh at which the solution of the governing equations was achieved. Then, a medium size and a finer meshes, which consisted of $110 \times 88 \times 88$ and $152 \times 120 \times 120$, respectively, were tested. It is important to mention that, for all these grids, a non-uniform mesh is made finer near the inlet and the axis. It was observed that the maximum difference between the predictions of the

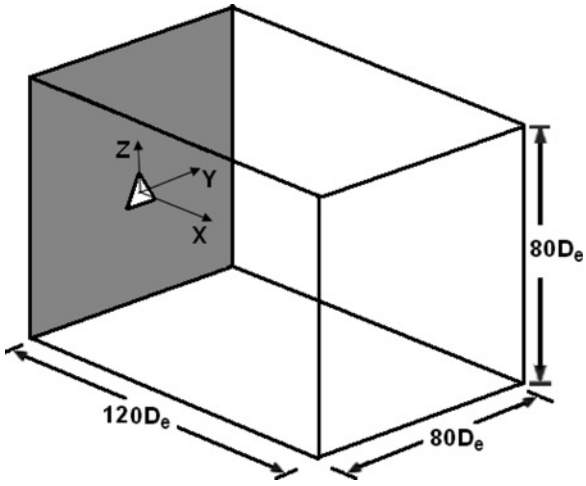

Figure 1.
Schematic of the triangular orifice geometry and the computational domain

medium and the fine meshes was 2.05 percent, which was found along the centerline. Therefore, in order to minimize the computational time, the medium mesh was used for all the simulations reported below. The computational grid is shown in Figure 2.

The solution of the governing equations was obtained by using the commercial CFD software, FLUENT version 6.1.22, which is based on finite volume formulation. The PISO (Issa, 1986) method was applied for the pressure-velocity coupling and the PRESTO (FLUENT, 2005) method was used for the pressure discretization. The QUICK (Leonard, 1979a) scheme was used for the convection terms in all transport equations. False-diffusion errors in numerical solutions of convection-diffusion problems arise from the numerical approximations of the convection term in the conservation equations (Patel, 1985). In contrast with the oscillatory or unstable second-order central-difference convection methods or artificially diffusive methods using upstream-weighted first-order differencing, the QUICK method is very stable for all flow regimes and highly accurate: global truncation error is uniformly third order for any combination of convection and diffusion (Leonard, 1979b). The solution convergence was assumed when all of the residuals parameters fell below 10^{-5} (Khademi Shamami, 2008).

3. Results and discussions

3.1 Mean-velocity field

Figures 3(a) and 3(b) present the decay of the streamwise mean velocity along the jet centerline up to $x/D_e = 60$ as predicted by the eddy-viscosity models, and Reynolds stress closures. The data in the near-field region are shown in Figure 4, providing a more detailed presentation of the jet features and results in this important region. The experimental data, which are obtained by using hot-wire anemometry are provided by Quinn (2005a), for which it is reported that the maximum uncertainty of the measurement is approximately 1 percent. U_{cl} is the local streamwise mean velocity on the jet centerline and U_{max} is the maximum value of the streamwise mean velocity on the jet centerline. In fact, U_{max} does not occur at the inlet and that is why U_{max}/U_{cl} is not

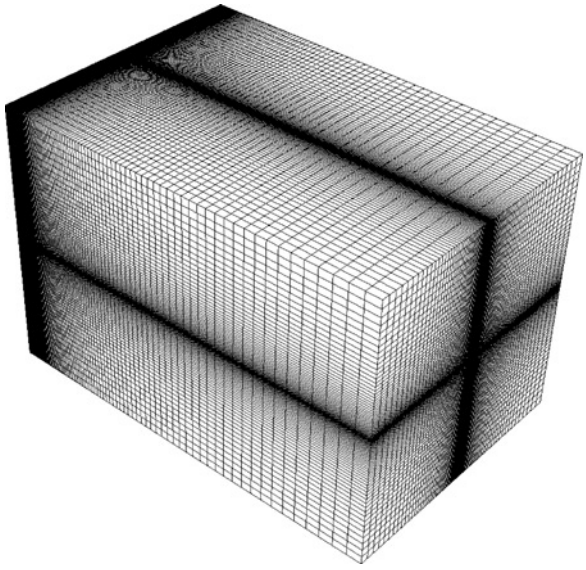

Figure 2.
The computational grid

equal to 1 at the exit of the jet, $x/D_e = 0$. The experimental data in Figure 3 and more evidently in Figure 4 show that the value of U_{max}/U_{cl} at the jet exit plane is greater than unity. This is attributed to the vena contracta effect associated with a sharp-edged orifice (Quinn, 2005a). Figure 4 shows clearly that all the tested turbulence RANS models are able to capture the vena contracta effect, i.e. the initial acceleration of the flow. Figure 4(a) reveals that among the two-equation eddy-viscosity models, the RKEM predictions in the jet near-field region, i.e. $0 < x/D_e < 10$, are in good agreement with the experimental data. However, it overpredicts noticeably the experimental data in the jet mid- and far-field regions, i.e. $x/D_e > 10$. It is still by far the best model in comparison with all the other two-equation eddy-viscosity models, which all exhibit a larger mean-velocity decay rate. In summary, the predictions of the KEM and the RNG in the near field, as shown in Figure 4(a), exhibit the highest and the lowest decay rate of the streamwise mean velocity along the jet centerline, respectively. This indicates that the KEM and the RNG predict the highest and the lowest jet mixing rate in the near-field region, respectively.

On the other hand, the Reynolds stress closures show far superior predictions compared to the two-equation eddy-viscosity models. Indeed, Figure 4(b) reveals that both the RSM and the SSG predict the streamwise mean-velocity decay of the jet in the near field extremely well, i.e. for $x/D_e < 10$. In the mid- and far-field regions, the RSM shows better predictions than the SSG model, although it still overpredicts slightly the experimental data, as shown in Figure 3(b). This figure shows that the deviation of the

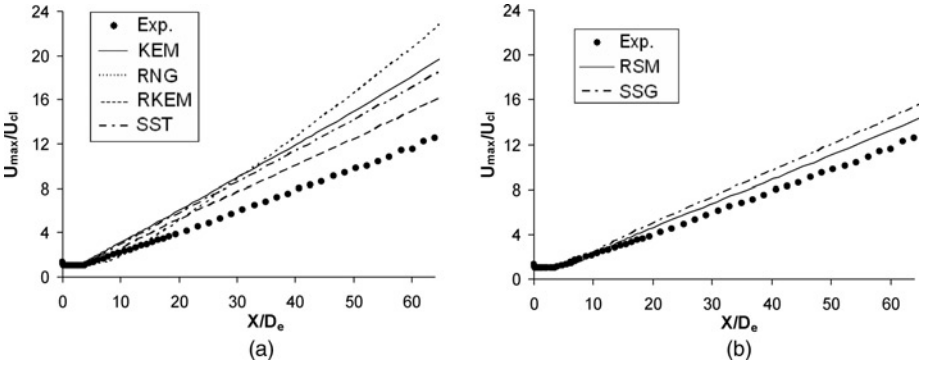

Figure 3.
Streamwise mean-velocity decay along the jet centerline: (a) eddy-viscosity models and (b) Reynolds stress closures

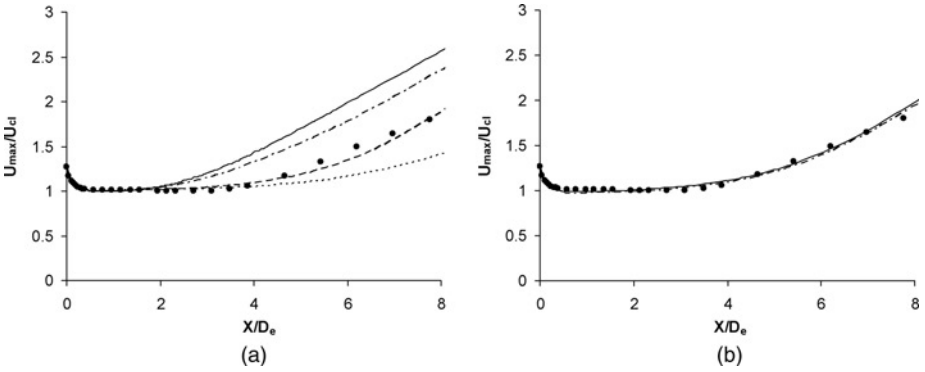

Figure 4.
Streamwise mean-velocity decay along the jet centerline in the near-field region: (a) eddy-viscosity models and (b) Reynolds stress closures

RSM predictions from the experimental data becomes quite noticeable in the jet far field, although it is still not very significant. For example, the predictions of the RSM are 14 percent higher than the corresponding experimental data at $x/D_e = 50$.

The normalized streamwise mean-velocity profiles along the central *x-y* and *x-z* jet planes at three typical downstream locations are presented in Figures 5 and 6, respectively. In general, the RSMs perform better than the two-equation eddy-viscosity

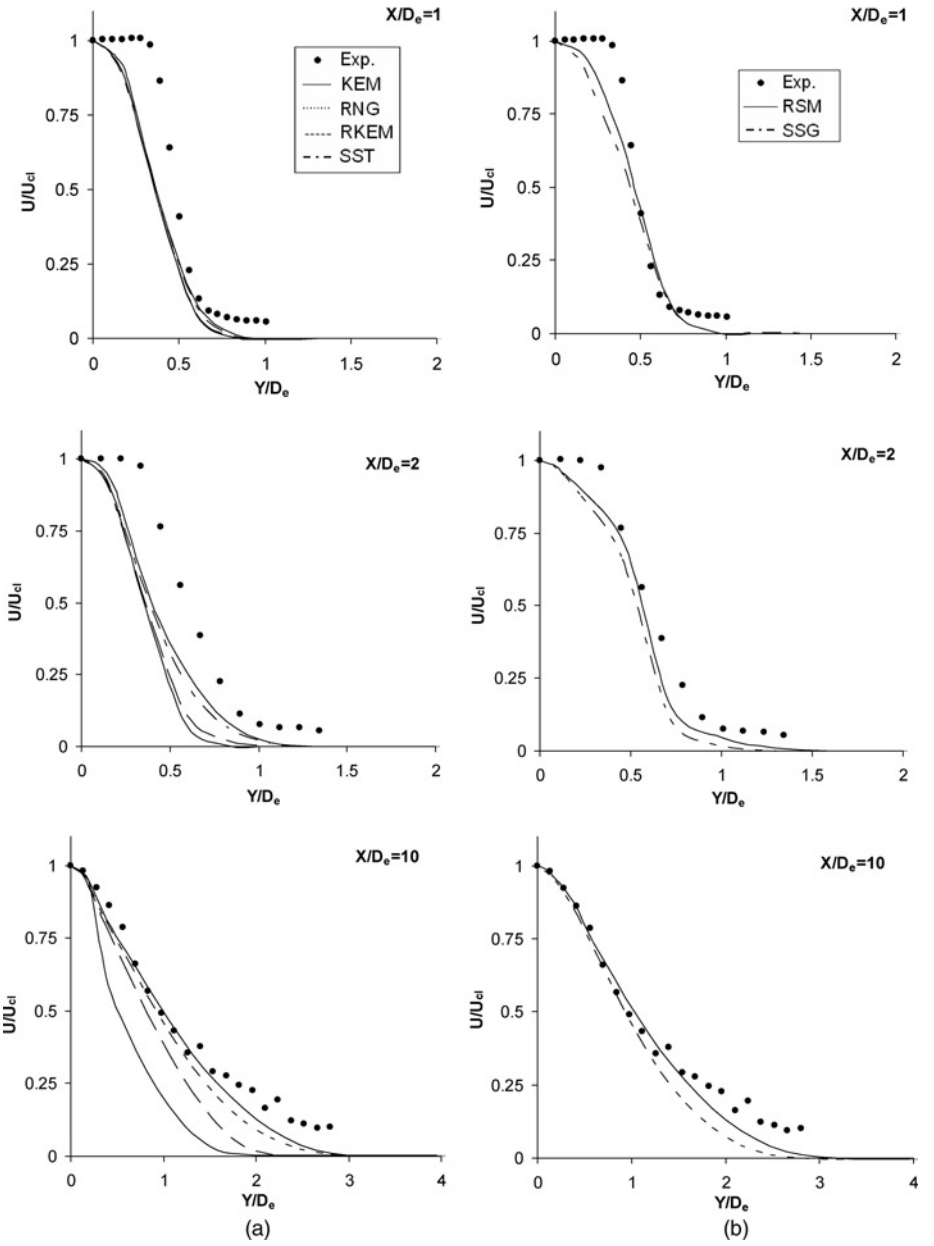

Figure 5.
Normalized streamwise mean-velocity profile in the central *x-y* plane: (a) eddy-viscosity models and (b) Reynolds stress closures

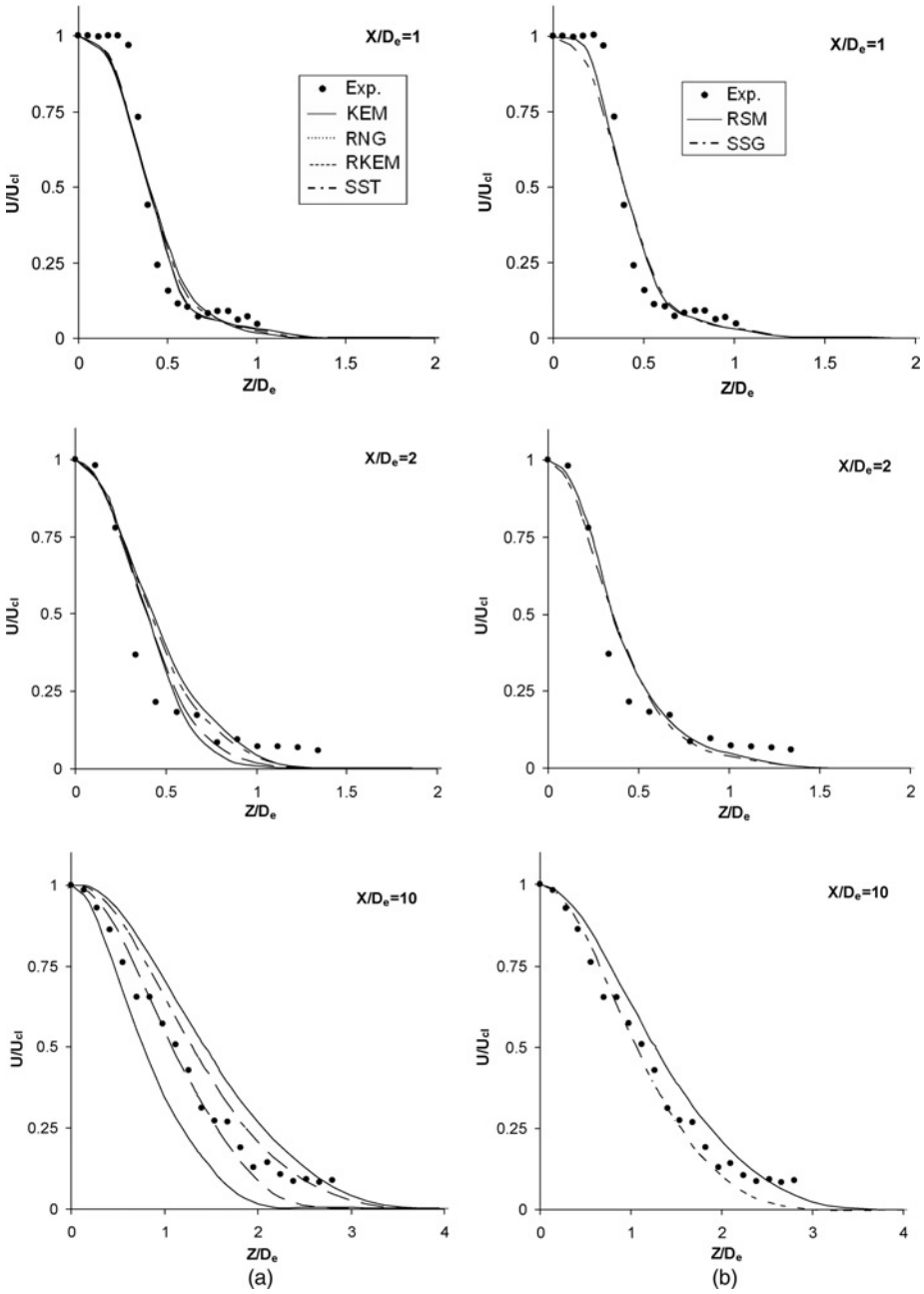

Figure 6.
Normalized streamwise mean-velocity profile in the central *x-z* plane: (a) eddy-viscosity models and (b) Reynolds stress closures

models. None of the models does a very good job of predicting the top-hat feature profile at $x/D_e = 1$ and 2 in the *x-y* plane, as shown in Figure 5, and at $x/D_e = 1$ in the *x-z* plane, as shown in Figure 6. Furthermore downstream the jet, the RSMs perform better with the SSG model showing slightly better agreement with the corresponding

experimental data. Both of these models and all the two-equation eddy-viscosity models under predict the experimental data especially for $y/D_e \geq 1.5$ at $x/D_e = 10$ (Figure 5).

In conclusion, the performance of the SSG model is better than those of the eddy-viscosity models. However, among all the tested RANS models, the RSM produced the best predictions in comparison with the experimental data.

The development of the jet half-velocity width (where $U/U_{cl} = 0.5$) along the centerline *x-y* and *x-z* jet planes, as shown in Figure 1, is presented in Figures 7 and 8, respectively. It is reported that the jet half-velocity width decreases initially, which is attributed to the vena contracta effect, then increases nearly linearly with the streamwise distance, as triggered by the large-scale structures emanating from the flat sides of the triangular orifice (Quinn, 2005a).

Figures 7(a) and 8(a), which compare the performance of the eddy-viscosity models in predicting the development of the jet half-velocity width, demonstrate that none of these closure models is capable of reproducing the experimental profiles. They either underpredict the jet half-velocity width in the *x-y* plane, or overpredict the jet half-velocity width in the *x-z* plane. The same remarks apply to the predictions of the SSG

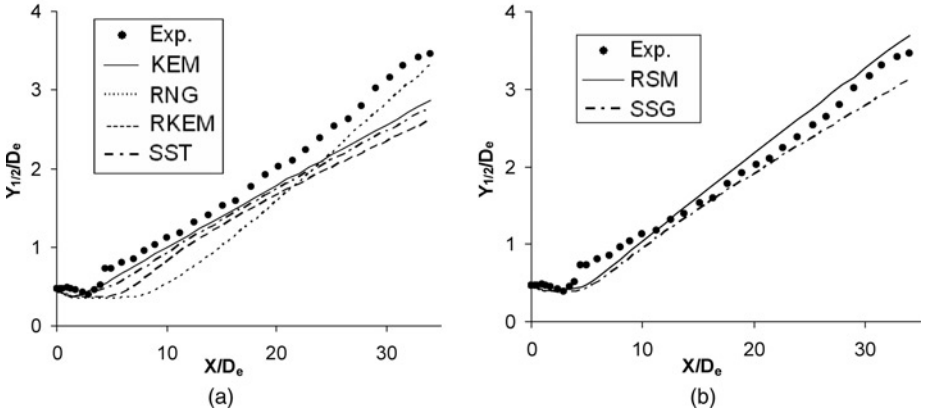

Figure 7.
Development of the jet half-velocity width in the central *x-y* plane: (a) eddy-viscosity models and (b) Reynolds stress closures

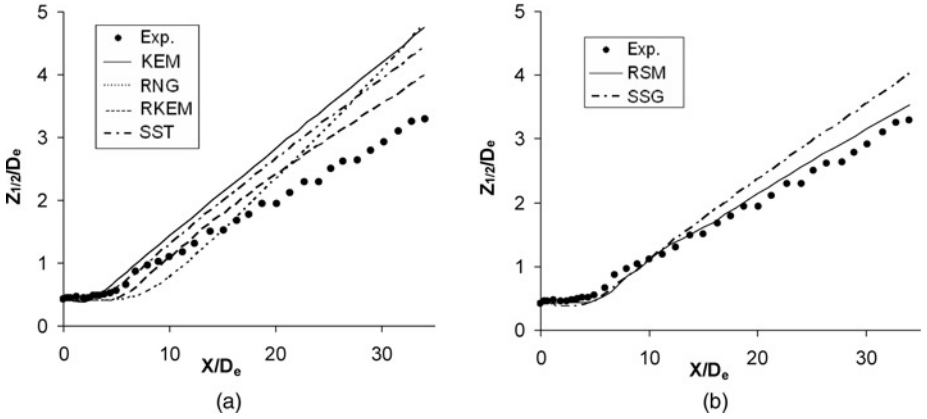

Figure 8.
Development of the jet half-velocity width in the central *x-z* plane: (a) eddy-viscosity models and (b) Reynolds stress closures

model, though with a less degree. The standard RSM, on the other hand, appears to be the only RANS closure which is capable of reproducing the experimental data fairly well.

Profiles of the geometric mean of the jet half-velocity widths, which is defined as $B_e = (Y_{1/2} \times Z_{1/2})^{0.5}$ (Quinn, 2005a), are shown in Figure 9. This quantity represents the overall spreading rate of a jet issuing from a non-circular orifice (or nozzle). Figure 9 shows clearly that the geometric mean of the jet half-velocity widths is well predicted by all the tested models, with the exception of the RNG which shows a very slow spreading rate up to $x/D_e = 20$ beyond which it exhibits a faster spreading rate. The KEM displays the highest magnitude of the half-velocity geometric mean jet width in the region $x/D_e < 25$. This corresponds to a prediction of a faster mixing rate in the jet near field compared to the other models. On the other hand, both the SSG and the RSM appear to reproduce the experimental data fairly well.

3.2 Turbulence quantities

Figure 10 shows the profiles of the three components of the normalized measured and predicted turbulence intensity along the jet centerline. This figure reveals a steep initial increase for all the three components of turbulence intensity, which is attributed to the production of turbulence from the mean flow shear in the shear layers emanating from the flat sides of the triangular orifice and diffusion of the turbulence from the shear layers to the jet centerline (Quinn, 2005a). The experimental data of all the normalized u', v', and w' show a peak along the centerline. Although all the eddy-viscosity models appear to be able to predict this peak, they overpredict its magnitude by a substantial amount when compared with the experimental data, especially for the lateral components (v' and w'). In addition, the majority of the eddy-viscosity closures seem incapable of predicting the exact axial location of the peak. The only exception concerns the predictions of the SST and RKEM models. The former is found able to nearly reproduce the experimental profiles of both u' and w' components profiles; whereas only the profile of v' component is correctly predicted by the latter model. It is important to note that the reason that the magnitude of these two components (v' and

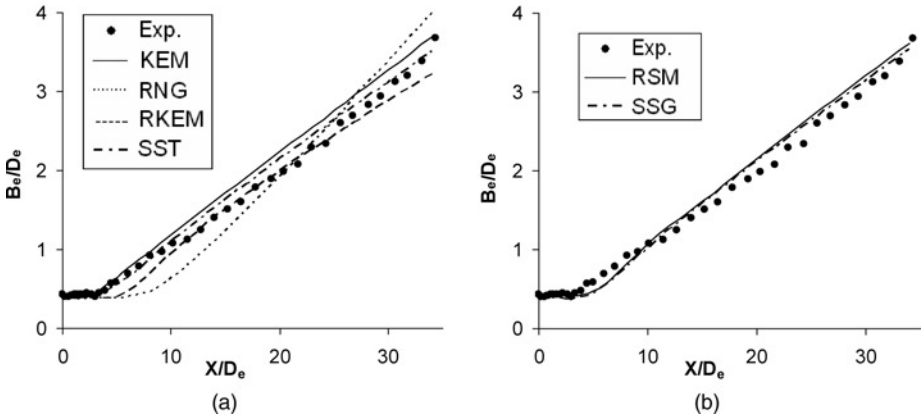

Figure 9.
Geometric mean of the jet half-velocity widths: (a) eddy-viscosity models and (b) Reynolds stress closures

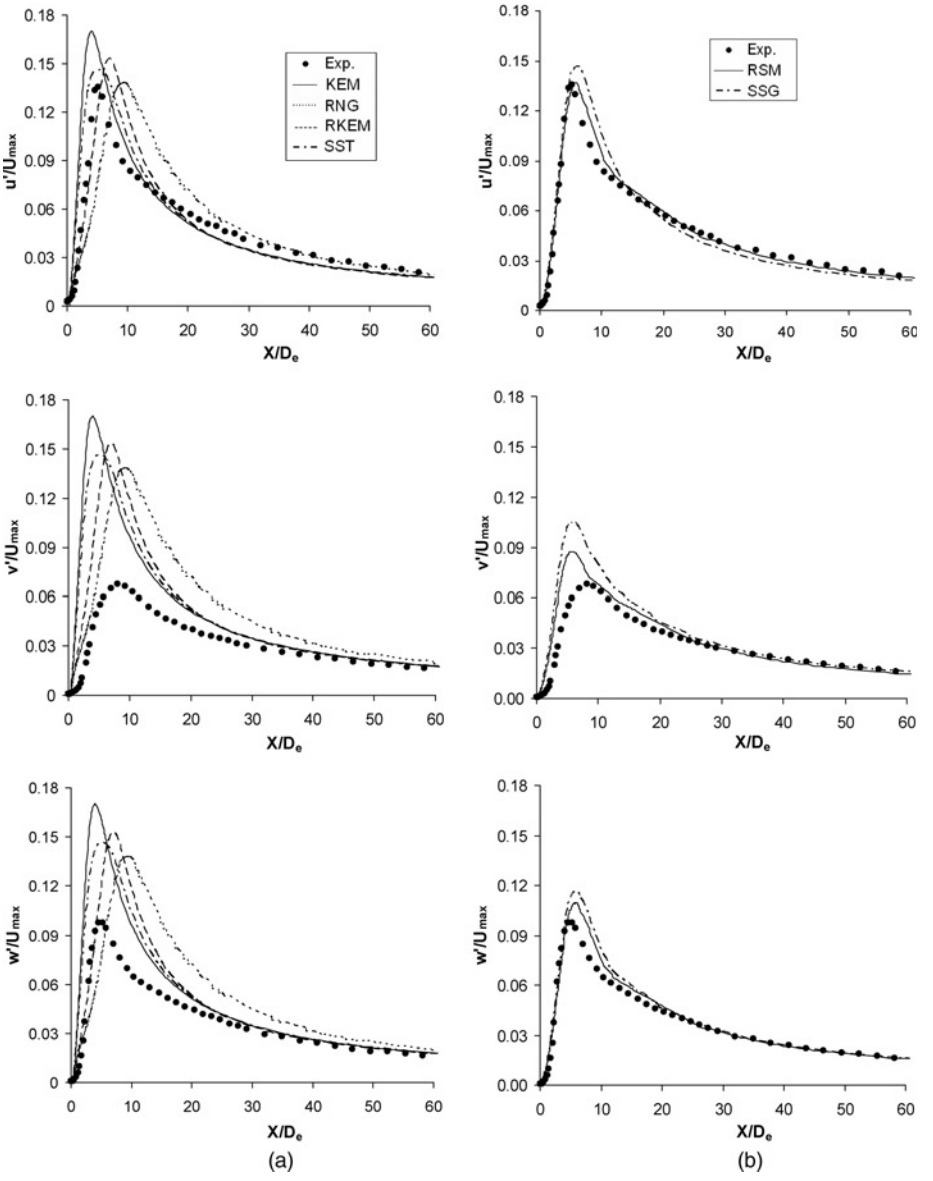

Figure 10.
Evolution of the normalized turbulence intensity components along the jet centerline: (a) eddy-viscosity models and (b) Reynolds stress closures

w') is inaccurately predicted by the eddy-viscosity closures is due to the fact that turbulence is strongly anisotropic, especially in the jet near- and mid-field regions. These models work better for less anisotropic turbulent flows.

On the other hand, the RSM and the SSG predictions of the streamwise, u', spanwise, v', and the lateral, w', turbulence intensity components, are generally in fair agreement with their experimental counterparts, with the RSM predictions showing slightly better agreement with the experimental data. The RSM prediction of the peak

in the spanwise turbulence intensity component, v', is also the best among these models.

4. Conclusions

The main findings of the present three-dimensional simulation of an equilateral triangular turbulent free jet, with a Reynolds number of 1.84×10^5 at the jet exit, can be summarized as follows. The two-equation eddy-viscosity turbulence closure models showed poor performance in predicting the jet streamwise mean-velocity decay and half-velocity width along the two lateral plans, as well as turbulence intensities profiles. This poor performance of the eddy-viscosity models is mainly caused by the anisotropic nature of jet turbulence. Among the eddy-viscosity models, the RKEM shows the best prediction of the streamwise mean-velocity decay along the jet centerline. On the other hand, both RSMs, i.e. RSM and SSG, exhibited much better performance than all tested eddy-viscosity closures. The standard RSM showed the best predictions for all the jet flow main features. Indeed, it appeared overall capable of reproducing the experimental flowfield profiles of the equilateral triangular turbulent free jet examined here. The only exception, which might be considered as a weakness but still insignificant, is its inability to capture accurately enough the flatness of the streamwise mean-velocity profile in the very near field of the centerline *x-y* plane.

References

Abdel-Hameed, H. and Bellan, J. (2002), "Direct numerical simulations of two-phase laminar jet flows with different cross-section injection geometries", *Physics of Fluids*, Vol. 14 No. 10, pp. 3655-74.

Berg, J.R., Ormiston, S.J. and Soliman, H.M. (2006), "Prediction of the flow structure in a turbulent rectangular free jet", *International Communications in Heat and Mass Transfer*, Vol. 33, pp. 552-63.

Choudhury, D. (1993), "Introduction to the renormalization group method and turbulence modeling", *Fluent Inc. Technical Memorandum TM-107*, Lebanon, NH.

Daly, B.J. and Harlow, F.H. (1970), "Transport equations in turbulence", *Physics of Fluids*, Vol. 13 No. 11, pp. 2634-49.

de With, G. and Holdo, A.E. (2005), "The use of turbulent inflow conditions for the modelling of a high aspect ratio jet", *Fluid Dynamics Research*, Vol. 37 No. 6, pp. 443-61.

FLUENT (2005), *FLUENT User's Guide*, Fluent Inc., Lebanon, NH.

Fu, S., Launder, B.E. and Leschziner, M.A. (1987), "Modeling strongly swirling recirculating jet flow with Reynolds-stress transport closures", *Proceedings of the Sixth Symposium on Turbulent Shear Flows*, *Toulouse*, pp. 17.6.1-6.

Gibson, M.M. and Launder, B.E. (1978), "Ground effects on pressure fluctuations in the atmospheric boundary layer", *Journal of Fluid Mechanics*, Vol. 86, pp. 491-511.

Grandmaison, E.W., Pollard, A. and Ng, S. (1991), "Scalar mixing in a free, turbulent rectangular jet", *International Journal of Heat and Mass Transfer*, Vol. 34 No. 10, pp. 2653-62.

Grinstein, F.F. (1998), "Vortex dynamics and transition to turbulence in low aspect-ratio rectangular free jets", FEDSM98-5307, American Society of Mechanical Engineers, Fluids Engineering Division (Publication), FED.

Grinstein, F.F. and DeVore, C.R. (1996), "Dynamics of coherent structures and transition to turbulence in free square jets", *Physics of Fluids*, Vol. 8 No. 5, pp. 1237-51.

Grinstein, F.F. and Kailasanath, K. (1995), "Three-dimensional numerical simulations of unsteady reactive square jets", *Combustion and Flame*, Vol. 100 Nos 1/2, pp. 2-10.

Gutmark, E.J. and Grinstein, F.F. (1999), "Flow control with noncircular jets", *Annual Review of Fluid Mechanics*, Vol. 31, pp. 239-72.

Gutmark, E., Schadow, K.C. and Wilson, K.J. (1991), "Subsonic and supersonic combustion using noncircular injectors", *Journal of Propulsion and Power*, Vol. 7 No. 2, pp. 240-9.

Gutmark, E., Schadow, K.C., Parr, T.P., Hanson-Parr, D.M. and Wilson, K.J. (1989a), "Noncircular jets in combustion systems", *Experiments in Fluids*, Vol. 7, pp. 248-58.

Gutmark, E., Schadow, K.C. and Wilson, K.J. (1989b), "Noncircular jet dynamics in supersonic combustion", *Journal of Propulsion and Power*, Vol. 5 No. 5, pp. 529-33.

Imine, B., Abidat, M., Imine, O., Gazzah, H. and Gokalp, I. (2004), "Study of turbulent variable density jets with different asymmetric geometries", *Proceedings of the Seventh Biennial Conference on Engineering Systems Design and Analysis*, Vol. 1, pp. 505-11.

Issa, R.I. (1986), "Solution of the implicitly discretized fluid flow equations by operator-splitting", *Journal of Computational Physics*, Vol. 62 No. 1, pp. 40-65.

Iyogun, O.C. and Birouk, M. (2008), Effect of exit velocity on entrainment and spreading of a jet issuing from an asymmetric nozzle with and without a sudden expansion, Paper AIAA-2008-765, 46th AIAA Aerospace Sciences Meeting and Exhibit, 7-10 January 2008, Reno, NV.

Iyogun, C.O. and Birouk, M. (2009), "Effects of sudden expansion on entrainment and spreading rates of a jet issuing from asymmetric nozzles", *Flow Turbulence and Combustion*, Vol. 82 No. 3, pp. 287-315.

Jiang, X. and Luo, K.H. (2001), "Direct numerical simulation of transitional noncircular buoyant reactive jets", *Theoretical and Computational Fluid Dynamics*, Vol. 15 No. 3, pp. 183-98.

Khademi, S.K. (2008), "Performance of RANS models for simulating turbulent swirling and free jet flows", MSc thesis, University of Manitoba, Winnipeg.

Kim, S.E. and Choudhury, D. (1995), "Near-wall treatment using wall functions sensitized to pressure gradient", *ASME, Fluids Engineering Division (FED), Separated and Complex Flows*, Vol. 217, pp. 273-80.

Krothapalli, A., Baganoff, D. and Karamcheti, K. (1981), "On the mixing of a rectangular jet", *Journal of Fluid Mechanics*, Vol. 107, pp. 201-20.

Launder, B.E. (1989a), "Second-moment closure and its use in modeling turbulent industrial flows", *International Journal for Numerical Methods in Fluids*, Vol. 9 No. 8, pp. 963-85.

Launder, B.E. (1989b), "Second-moment closure: present and future?", *International Journal of Heat and Fluid Flow*, Vol. 10 No. 4, pp. 282-300.

Launder, B.E. and Spalding, D.B. (1972), *Lectures in Mathematical Models of Turbulence*, Academic Press, London.

Launder, B.E. and Spalding, D.B. (1974), "The numerical computation of turbulent flows", *Computer Methods in Applied Mechanics and Engineering*, Vol. 3 No. 2, pp. 269-89.

Launder, B.E., Reece, G.J. and Rodi, W. (1975), "Progress in the development of a Reynolds-stress turbulence closure", *Journal of Fluid Mechanics*, Vol. 68, pp. 537-66.

Leonard, B.P. (1979a), "A stable and accurate convective modeling procedure based on quadratic upstream interpolation", *Computer Methods in Applied Mechanics and Engineering*, Vol. 19 No. 1, pp. 59-98.

Leonard, B.P. (1979b), "The QUICK finite difference method for the convection-diffusion equation", *Advances in Computer Methods for Partial Differential Equations – III; Proceedings of the Third International Symposium*, pp. 292-7.

Lien, F.S. and Leschziner, M.A. (1994), "Assessment of turbulent transport models including non-linear RNG eddy-viscosity formulation and second-moment closure for flow over a backward-facing step", *Computers and Fluids*, Vol. 23 No. 8, pp. 983-1004.

Liu, H. and Wu, S. (1995), "Enhanced mixing of 2D lobed nozzles", *Proceedings of the International Gas Turbine and Aeroengine Congress and Exposition, ASME 95-GT–339*.

Mahmud, T., Sangha, S.K., Costa, M. and Santos, A. (2007), "Experimental and computational study of a lifted, non-premixed turbulent free jet flame", *Fuel*, Vol. 86 Nos 5/6, pp. 793-806.

Marsters, G.F. (1981), "Spanwise velocity distributions in jets from rectangular slots", *AIAA Journal*, Vol. 19 No. 2, pp. 148-52.

Menter, F.R. (1994), "Two-equation eddy-viscosity turbulence models for engineering applications", *AIAA Journal*, Vol. 32 No. 8, pp. 1598-605.

Menter, F.R., Kuntz, M. and Langtry, R. (2003), "Ten years of industrial experience with the SST turbulence model", *Fourth International Symposium on Turbulence, Heat and Mass Transfer*, pp. 625-32.

Mi, J., Deo, R.C. and Nathan, G.J. (2005), "Characterization of turbulent jets from high-aspect-ratio rectangular nozzles", *Physics of Fluids*, Vol. 17 No. 6, pp. 1-4.

Mi, J., Nathan, J. and Luxton, R.E. (2000), "Centerline mixing characteristics of jets from nine differently shaped nozzles", *Experiments in Fluids*, Vol. 28 No. 1, pp. 93-4.

Miller, R.S., Madnia, C.K. and Givi, P. (1995), "Numerical simulation of non-circular jets", *Computers and Fluids*, Vol. 24 No. 1, pp. 1-25.

Patel, M.K., Markatos, N.C. and Cross, M. (1985), "Method of reducing false-diffusion errors in convection-diffusion problems", *Applied Mathematical Modelling*, Vol. 9 No. 4, pp. 302-6.

Quinn, W.R. (1990), "Mean flow and turbulence measurements in a triangular turbulent free jet", *International Journal of Heat and Fluid Flow*, Vol. 11 No. 3, pp. 220-4.

Quinn, W.R. (1992), "Turbulent free jet flows issuing from sharp-edged rectangular slots. The influence of slot aspect ratio", *Experimental Heat Transfer*, Vol. 5 No. 2, pp. 203-15.

Quinn, W.R. (1994), "Development of a large-aspect-ratio rectangular turbulent free jet", *AIAA Journal*, Vol. 32 No. 3, pp. 547-54.

Quinn, W.R. (2005a), "Near-field measurements in an equilateral triangular turbulent free jet", *AIAA Journal*, Vol. 43 No. 12, pp. 2574-85.

Quinn, W.R. (2005b), "Measurements in the near flow field of an isosceles triangular turbulent free jet", *Experiments in Fluids*, Vol. 39 No. 1, pp. 111-26.

Quinn, W.R. (2005c), "Phase-averaged measurements in an isosceles triangular turbulent free jet", *Experiments in Fluids*, Vol. 39, pp. 941-3.

Quinn, W.R. and Militzer, J. (1988), "Experimental and numerical study of a turbulent free square jet", *Physics of Fluids*, Vol. 31 No. 5, pp. 1017-25.

Reddy, D.R., Steffen, C.J. Jr. and Zaman, K.B.M.Q. (1998), "Computation of 3-D compressible flow from a rectangular nozzle with delta tabs", *American Society of Mechanical Engineers, Proceedings of the 1997 International Gas Turbine & Aeroengine Congress & Exposition, Paper 97-GT-257*.

Reddy, D.R., Steffen, C.J., Jr. and Zaman, K.B.M.Q. (1999), "Computation of three-dimensional compressible flow from a rectangular nozzle with delta tabs", *Journal of Engineering for Gas Turbines and Power*, Vol. 121 No. 2, pp. 235-42.

Rembold, B., Adams, N.A. and Kleiser, L. (2002), "Direct numerical simulation of a transitional rectangular jet", *International Journal of Heat and Fluid Flow*, Vol. 23 No. 5, pp. 547-53.

Rice, E.J. and Raman, G. (1993), "Supersonic jets from bevelled rectangular nozzles", *Proceedings of the ASME Winter Conference, 93-WA/NCA-26*, pp. 1-7.

Schadow, K.C., Gutmark, E., Parr, D.M. and Wilson, K.J. (1988), "Selective control of flow coherence in triangular jets", *Experiments in Fluids*, Vol. 6 No. 2, pp. 129-35.

Sfeir, A.A. (1979), "Investigation of three-dimensional turbulent rectangular jets", *AIAA Journal*, Vol. 17 No. 10, pp. 1055-60.

Sforza, P.M., Steiger, M.H. and Trentacoste, N. (1966), "Studies on three-dimensional viscous jets", *AIAA Journal*, Vol. 4 No. 5, pp. 800-6.

Shih, T.H., Liou, W.W., Shabbir, A., Yang, Z. and Zhu, J. (1995), "A new k-ε eddy-viscosity model for high Reynolds number turbulent flows", *Computers and Fluids*, Vol. 24 No. 3, pp. 227-38.

Speziale, C.G., Sarkar, S. and Gatski, T.B. (1991), "Modelling the pressure-strain correlation of turbulence: an invariant dynamical systems approach", *Journal of Fluid Mechanics*, Vol. 227, pp. 245-72.

Teshima, K. (1989), "Three-dimensional structure of a supersonic free jet issuing from a rectangular orifice", *Collection of Technical Papers ISCFD NAGOYA*, pp. 1144-9.

Tsuchiya, Y., Horikoshi, C., Sato, T. and Takahashi, M. (1989), "A study on the spread of rectangular jets. The mixing layer near the jet exit and visualization by the dye method", *JSME International Journal, Series II (Fluids Engineering, Heat Transfer, Power, Combustion, Thermophysical Properties)*, Vol. 32 No. 1, pp. 11-8.

Vandsburger, U. and Ding, C. (1995), "Spatial modulation of a forced triangular jet", *Experiments in Fluids*, Vol. 18 No. 4, pp. 239-48.

Wilson, R.V. and Demuren, A.O. (1998), "Numerical simulation of turbulent jets with rectangular cross-section", *Journal of Fluids Engineering*, Vol. 120 No. 2, pp. 285-90.

Wilson, W.M. and Imber, R.D. (2003), "CFD analyses of compact, high aspect ratio ejectors", *Proceedings of the ASME Fluids Engineering Division Summer Meeting*, Vol. 1, pp. 7-13.

Yakhot, V. and Orszag, S.A. (1986), "Renormalization group analysis of turbulence: I. Basic theory", *Journal of Scientific Computing*, Vol. 1 No. 1, pp. 3-51.

Yakhot, V., Orszag, S.A., Thangam, S., Gatski, T.B. and Speziale, C.G. (1992), "Development of turbulence model for shear flows by a double expansion technique", *Physics of Fluids A (Fluid Dynamics)*, Vol. 4 No. 7, pp. 1510-20.

Zaman, K.B.M.Q. (1995), "Spreading characteristics and thrust of jets from asymmetric nozzles", *NASA Technical Memorandum* No. 107132, pp. 1-19.

Zaman, K.B.M.Q. (1996), "Axis switching and spreading of an asymmetric jet: the role of coherent structure dynamics", *Journal of Fluid Mechanics*, Vol. 316, pp. 1-27.

Zaman, K.B.M.Q. (1999), "Spreading characteristics of compressible jets from nozzles of various geometries", *Journal of Fluid Mechanics*, Vol. 383, pp. 197-228.

Zaman, K.B.M.Q., Steffen, C.J. and Reddy, D.R. (1997), "Entrainment and spreading characteristics of jets from asymmetric nozzles", *AIAA-97-1878*, Vol. 99 No. 2, pp. 1-12.

Further reading

Patankar, S.V. (1980), *Numerical Heat Transfer and Fluid Flow*, Hemisphere, Washington, DC.

About the authors

Keivan Khademi Shamami is a graduate student in the Department of Mechanical and Manufacturing Engineering, University of Manitoba, Canada. His current research project includes numerical simulation of swirling flows and turbulent free jets.

Madjid Birouk is Associate Professor of Mechanical and Manufacturing Engineering, University of Manitoba, Canada. His current research focuses on combustion, reacting and non-reacting swirling flows, diffusion flames, droplet and spray evaporation and combustion, turbulence, and Turbulent jet flows. Madjid Birouk is the corresponding author and can be contacted at: biroukm@cc.umanitoba.ca